Intraseasonal Variability of the Zonal-Mean Extratropical Tropopause: The Role of Changes in Polar Vortex Strength and Upper-Troposphere Wave Breaking

JESÚS Á. BARROSO

Universidad Complutense de Madrid, Madrid, Spain

PABLO ZURITA-GOTOR

Universidad Complutense de Madrid, and Instituto de Geociencia, Centro Mixto del Consejo Superior de Investigaciones Científicas–Universidad Complutense de Madrid, Madrid Spain

(Manuscript received 1 July 2015, in final form 15 December 2015)

ABSTRACT

A principal component analysis of the Northern Hemisphere extratropical zonal-mean tropopause variability at intraseasonal time scales is presented in this work. Wavy deformations of the tropopause dominate this variability and explain significantly more variance than changes in the extratropical-mean tropopause height. The first mode is well correlated with the zonal index. Analysis of the dynamical evolution of the modes shows that tropopause deformations are caused by anomalous wave breaking at the tropopause level occurring in a preexisting anomalous stratospheric polar vortex. Specifically, an intense (weak) polar vortex is associated with a rising (sinking) of the polar tropopause, while anomalous wave breaking in the midlatitudes produces a dipolar tropopause change that is consistent with the anomalous meridional eddy flux of quasigeostrophic potential vorticity. These two forcings operate on different time scales and can be separated when the data are filtered at high or low frequency. Baroclinic equilibration seems to play a small role in the extratropical internal tropopause variability and the impact of tropospheric and stratospheric dynamics is quantitatively similar. A similar analysis for the Southern Hemisphere extratropics displays the same qualitative behavior.

1. Introduction

The tropopause is one of the most prominent features of the atmospheric structure, playing a fundamental role both as a dynamical boundary between an active troposphere with short response times and a much quieter stratosphere and as a material boundary between the well-mixed troposphere and the stratified stratosphere. Despite this important role, there is no unique, fundamental way to define the tropopause but several empirical criteria based on properties known to experience a steep change when moving from the troposphere to the stratosphere, such as lapse rate (WMO 1957), potential vorticity (Reed 1955; Hoinka 1998), or tracer abundance (Bethan et al. 1996). Lacking a fundamental definition for the tropopause, some ambiguity may arise when studying the determination and/or variability of the tropopause, as the relative importance of the processes involved might depend on the framework used.

The determination of the mean tropopause is a classical problem in general circulation theory. The simplest model regards the tropopause as the boundary between a radiative-equilibrium stratosphere and a troposphere in some form of dynamical equilibrium, typically convective or baroclinic (Held 1982; Lindzen 1993). Although highly idealized, this model can explain the change in lapse rate (between dynamically adjusted and radiative-equilibrium values), potential vorticity (assuming eddies greatly homogenize potential vorticity in the troposphere), and chemical species (owing to the enhanced static stability and weak mixing in the stratosphere) across the tropopause. The requirement that the stratosphere is in radiative equilibrium poses a constraint on tropopause height (the so-called radiative constraint), as the outgoing radiative flux at this level is then determined by the net

Corresponding author address: Jesús Á. Barroso, Departamento de Geofísica y Meteorología I, Facultad de Ciencias Físicas, Universidad Complutense de Madrid, Plaza de Ciencias, 1, 28040 Madrid, Spain. E-mail: jesusangelbarroso@ucm.es

DOI: 10.1175/JAS-D-15-0177.1

column heating. The main limitation of this model is that the assumption of a stratosphere in radiative equilibrium is not well satisfied, as it is known that the polar stratosphere, especially in winter, is far from radiative equilibrium because of the dynamical warming by the residual circulation (Holton et al. 1995), which is expected to influence tropopause height (Appenzeller et al. 1996; Thuburn and Craig 2000; Birner 2010). Nevertheless, Zurita-Gotor and Vallis (2011) have argued that a tight radiative constraint may still constrain the sensitivity of tropopause height to dynamical forcing, consistent with the good agreement found by Thuburn and Craig (1997) in atmospheric model simulations.

To close the problem, additional assumptions must be made about the tropospheric dynamical equilibrium, for which different dynamical arguments have been proposed. These closures generally fall in two categories: some are based on dry eddy equilibration theories like baroclinic adjustment (Held 1982; Schneider 2004; Bordi et al. 2004), while others are based on moist convection (Juckes 2000; Wu and Pauluis 2014). Motivated by these ideas, previous observational studies of intraseasonal tropopause variability (Dell'Aquila et al. 2006; Son et al. 2007) have sought a connection between changes in eddy activity and in tropopause height, assuming that on short time scales the eddy fluxes drive the tropopause away from equilibrium during baroclinic life cycles.

Based on the lapse rate definition, a warming in the upper troposphere and/or a cooling in the lower stratosphere will raise the tropopause, and vice versa (Shepherd 2002). This seems to be the case for synoptic and monthly variability of the tropopause, both of which are characterized by high correlations with opposite sign at levels above and below the tropopause (Seidel and Randel 2006); a similar potential temperature dipole was also found by Son et al. (2007) for the intraseasonal variability of the zonal-mean tropopause. This pattern is expected to be produced by dynamically balanced circulations characteristic of cyclones and anticyclones in the case of synoptic variability (Seidel and Randel 2006; Zängl and Wirth 2002) and to the accumulated effects of the synoptic variability in the case of monthly variability (Seidel and Randel 2006).

Yet despite all of these studies, a systematic analysis of the variability of the zonal-mean tropopause is still lacking. We are unaware in particular of any previous work discussing the leading modes of intraseasonal extratropical tropopause variability and their dynamics, although principal component analysis has been previously applied to tropopause height variability on interannual time scales (Wong and Wang 2003). While local variations in tropopause height are expected to be dominated by tropopause deformations on synoptic scales (Hoskins et al. 1985), the driving of the zonal-mean tropopause variability is not as obvious and different mechanisms may contribute to that variability. We can conceive two different scenarios. If baroclinic equilibration played the dominant role for tropopause variability, one might expect this variability to be driven by changes in eddy heat fluxes and by tropospheric baroclinic dynamics. Alternatively, tropopause variability might be associated with changes in the barotropic flow and with adjustment to balance accompanying the surface pressure changes associated with the annular mode variability (Thompson and Wallace 2000). In that scenario, stratospheric dynamics might also be important (Son et al. 2007) and eddy momentum fluxes may play a more important role than eddy heat fluxes in the troposphere.

This work investigates the spatial and temporal structure of zonal-mean thermal tropopause variability in the extratropics and its underlying dynamics using principal component analysis and lagged composites. The paper is organized as follows. Section 2 introduces the dataset and the methodology used for the statistical analysis. Section 3 presents the patterns associated with the leading modes of variability of the zonal-mean tropopause and section 4 analyzes the dynamics of these modes by means of composite Eliassen–Palm diagrams. Section 5 briefly performs a similar analysis for the Southern Hemisphere and section 6 summarizes the main conclusions of our study.

2. Data and methodology

For this study, gridded daily data from NCEP–NCAR Reanalysis-1 during the period 1978–2010 have been used, including daily tropopause pressure. To study the variability of tropopause height, this daily tropopause pressure was converted into tropopause height using cubic spline interpolation of the daily geopotential height data at the reference pressure levels. The seasonal cycle, defined as the first four harmonics of the daily climatology (Lorenz and Hartmann 2001), was removed from the daily data; then, interannual variability was eliminated by filtering the deseasonalized data using a Lanczos filter with 31 coefficients. To assess the robustness of the results, data from ERA-Interim were also used. In this case, the daily tropopause pressure was obtained applying the method of Reichler et al. (2003) to daily vertical temperature profiles.

The main focus of this work is the intraseasonal scale, though our results also hold at intraannual scales. Specifically, variability during the extended winter (from November to March in the Northern Hemisphere, from June to October in the Southern Hemisphere) is analyzed (which corresponds to 151 and 153 days yr^{-1},

respectively, making a total of 4983 and 5049 days for the 33 years included in the study).

Principal component analysis (PCA) was performed on the anomalous zonal-mean tropopause height field, with data weighted to account for the decrease of mass toward the pole (North et al. 1982b). One potential complication when studying the modes of variability of the extratropical tropopause is the confounding effect of extratropical incursions of tropical air with large tropopause height anomalies, together with the strong seasonal cycle in the meridional extension of the Hadley cell. Hence, we defined the extratropical northern region using a conservative latitude of 32.5°N, which seems to be the maximum northward extension of the tropical belt during the northern winter (Davis and Birner 2013). This range of latitudes may include some variability associated to the subtropical jet. Composite maps are used to analyze the growth and decay of the tropopause anomalies, averaging independent events (separated at least 7 days) exceeding one standard deviation of the reference time series. To assess the statistical significance of these maps, two-tailed t tests for the difference of means between the full and composite time series are performed using a confidence level of 0.99. Lag-composite maps are also used to analyze the plausible mechanisms that give rise to the anomalies in tropopause height. When covariances are employed, the statistical significance is assessed using a two-tailed t test on the correlation, taking into account the effective number of degrees of freedom implied by the time series autocorrelations. Following Bretherton et al. (1999), if X and Y are two time series with autocorrelations ρ^X and ρ^Y respectively, and N degrees of freedom, the effective number of degrees of freedom for statistical significance is given by

$$N_{\text{eff}}^{XY} = \frac{N}{\sum_{\nu=-(N-1)}^{(N-1)} (1 - |\nu|/N)\rho_\nu^X \rho_\nu^Y},$$

where ρ_ν^j is the autocorrelation of series j at lag ν.

3. Intraseasonal variability of the northern extratropical tropopause

As shown in Fig. 1, the first mode of variability of the northern extratropical zonal-mean tropopause during the extended winter has a dipole structure with the node around 50°N and extrema at 35° and 65°N. The second mode corresponds to a tripole pattern with nodes at 45° and 65°N; the two modes are uncorrelated at all lags and well separated according to the North et al. (1982a) criterion when the effective number of degrees of freedom for the time series is taken into account. This structure is characteristic of many extratropical fields—for example, the zonal-mean zonal wind (Lorenz and Hartmann 2001, 2003), the sea level pressure, and the geopotential height (Thompson and Wallace 2000). This type of variability is generally described as an annular mode (zonal index in the case of the zonal wind, Arctic Oscillation in the case of the geopotential height), which physically represents a mass fluctuation between the poles and midlatitudes with a high degree of zonal symmetry (Thompson and Wallace 2000), related to meridional displacements of the extratropical jet around its mean position (Lorenz and Hartmann 2003; Wittman et al. 2005) driven by interactions between the mean flow and the eddies. The relationship between the leading tropopause mode and the zonal index or the Arctic Oscillation will be discussed below. We also show in Fig. 1 the leading two modes calculated using ERA-Interim data. It can be seen that the patterns are quite similar to NCEP–NCAR reanalyses, though the polar center of action in EOF1 is weaker in ERA-Interim than in NCEP–NCAR reanalyses. Additionally, the first mode explains more variance for ERA-Interim than for NCEP–NCAR reanalyses. The large correlations between the modes independently calculated for both reanalyses [0.88 for both principal components (PCs)] demonstrate that these modes are robust in both datasets. The dynamical analysis in the next section uses NCEP–NCAR reanalyses data but results are similar with ERA-Interim.

Although the modes of variability are obtained from the zonally averaged tropopause height, we can look at the 2D structure by compositing the expansion coefficients, PC, with the complete field (Fig. 2). As expected there is great zonal symmetry, especially for EOF2 (Fig. 2b), though some minor asymmetries stand out for the first mode: a high tropopause over the oceanic storm tracks and a low tropopause over Iceland (which, together with the anomaly to the west of Canada, produce the tropopause height minimum at 65°N). However, this annular pattern only represents the average of many nonsymmetrical cases, while individual snapshots are dominated by wavy patterns as typically found in isentropic potential vorticity maps (Hoskins et al. 1985).

These modes of variability are highly insensitive to both the spatial and temporal ranges chosen for the analysis. In particular, the same modes are obtained when PCA is performed on the summer months or on the entire year although the explained variances vary (both modes explain more variance during the winter months than during the summer months or the whole year). From this, it can be concluded that the variability associated with these modes is representative of the intraannual variability of the extratropical zonal-mean

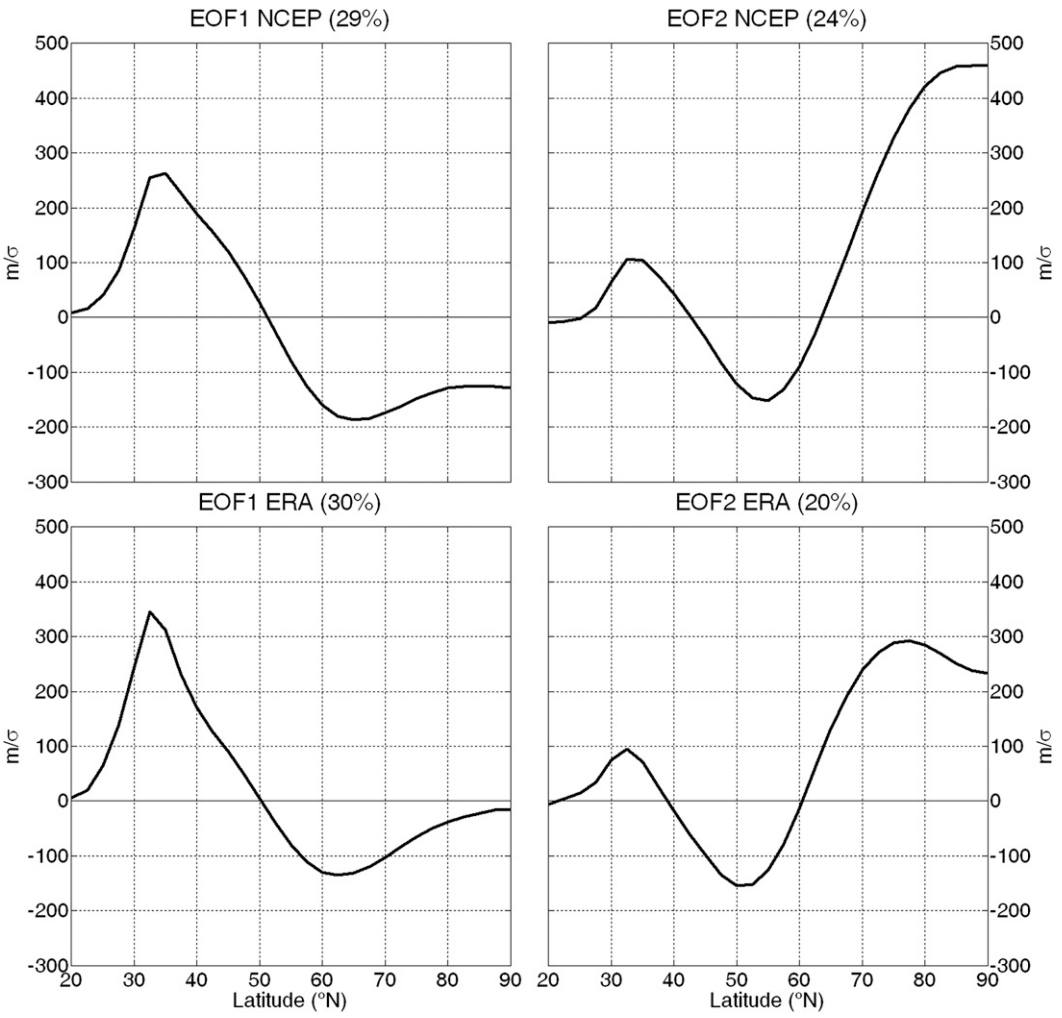

FIG. 1. Regression maps of anomalous zonal-mean tropopause height (m) on (left) PC1 and (right) PC2 for the (top) NCEP–NCAR Reanalysis-1 and (bottom) ERA-Interim datasets, during the extended NH winter.

tropopause. As for the robustness of the patterns to the choice of latitudinal band, the first mode emerges as long as midlatitudes (30°–40°N) are included in the analysis and is insensitive to the northern boundary of the domain; this suggests that its structure (a dipole centered at 50°N) is characteristic of the variability of the tropopause and not an artifact of the region chosen for the study. When the midlatitudes are not included in the PCA, there is a permutation between the first two modes and the tripole becomes the leading mode of variability. This mode is robust as long as polar latitudes are included in the analysis, no matter where the southern edge lies. This suggests that the first mode is basically a phenomenon originating in midlatitudes, while the second mode may be more related to polar variability. The more the latitude range is restricted to one of the two areas (either mid- or high latitudes) the more dominant the corresponding mode is (see Table 1).

4. Dynamical evolution of tropopause anomalies

a. Composite eddy forcing

Variations in midlatitude tropopause height are expected to be caused or at least associated with variations in the eddy activity (Dell'Aquila et al. 2006; Son et al. 2007). We describe changes in eddy activity using anomalous Eliassen–Palm (EP) fluxes and divergence, defined as

$$F_{(\varphi)} = -a\cos\varphi\,\overline{u'v'} \quad \text{and}$$
$$F_{(p)} = fa\cos\varphi\,\frac{\overline{v'\theta'}}{\overline{\theta}_p}, \tag{1}$$

where a is the radius of Earth, φ is the latitude, the prime denotes deviations from the zonal mean, the overbar denotes a zonal mean, and the subscript p denotes

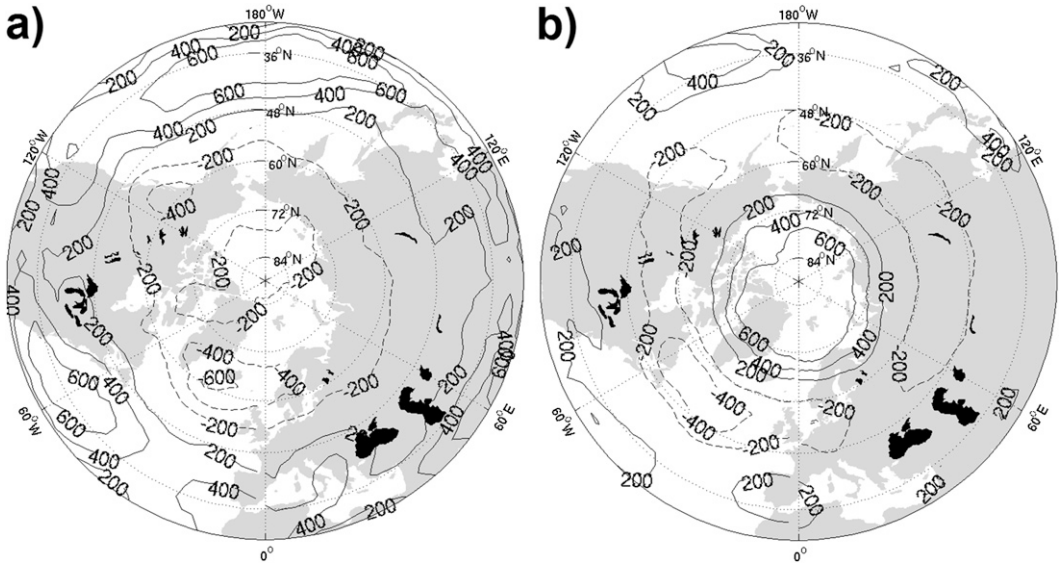

FIG. 2. Regression maps of anomalous tropopause height (m) on (a) PC1 and (b) PC2, during the extended NH winter.

derivative in the pressure coordinate; the rest of the notation is standard. The graphical convention of Edmon et al. (1980) for the representation of the divergence on the (φ, p) plane is used. The quasigeostrophic approximation is applied for reasons of simplicity; the results are unchanged when all the terms in the equations are included (not shown). In the analysis that follows, we discriminate between the planetary eddy forcing (by eddies with zonal wavenumber $k = 3$ or less) and the forcing by baroclinic waves of shorter scales ($k \geq 4$). We refer to the latter as the synoptic eddy forcing for consistency with Son et al. (2007), even though this term includes contributions by eddies of a wide range of scales, including longer-than-synoptic eddies.

As can be seen in Fig. 3, the perturbation in tropopause height associated with PC1 is preceded a few days earlier by an upward burst of synoptic waves at low latitudes, which propagate southward at tropopause levels and break near the subtropical jet. This produces a pattern of anomalous divergence (convergence) of the EP flux in the midlatitudes (in the subtropics), which accelerates the zonal-mean zonal wind on the northern flank of the extratropical jet and decelerates the zonal wind in the subtropics, shifting the extratropical jet northward. The planetary waves produce a similar dipolar pattern of Eliassen–Palm divergence at tropopause levels, except that enhanced vertical propagation into the stratosphere also reinforces the positive center on the northern side of the extratropical jet in this case. The subsequent wave breaking in the stratosphere leads to a deceleration of the stratospheric jet (Andrews et al. 1987) a few days later. The anomalies in the Eliassen–Palm divergence evolve quite rapidly. For positive lags, increased synoptic wave breaking to the north of the extratropical jet damps the anomaly on the zonal-mean zonal wind, while the decay of planetary waves ceases the forcing on the stratospheric jet and also contributes to the return of the extratropical jet to its mean position (albeit to a lesser extent than synoptic waves).

The anomalies in the EP flux divergence described above are consistent with the structure of the tropopause anomalies for this mode, which can be understood

TABLE 1. Variance explained by each of the first two modes of variability of the extratropical zonal-mean tropopause height for selected latitudinal ranges. Boldface (italics) indicates that the corresponding mode is highly correlated (and has a similar structure) with the ''midlatitude'' (''polar'') mode shown in Fig. 1 (top).

	PC1 (%)	PC2 (%)
20°–90°N	**28**	*20*
20°–80°N	**31**	*20*
20°–70°N	**36**	19
20°–60°N	**40**	18
20°–50°N	**46**	21
20°–40°N	**57**	21
20°–30°N	71	19
30°–90°N	**29**	*22*
40°–90°N	*33*	**26**
50°–90°N	*40*	**27**
60°–90°N	*49*	**31**
70°–90°N	*68*	**25**
80°–90°N	91	9

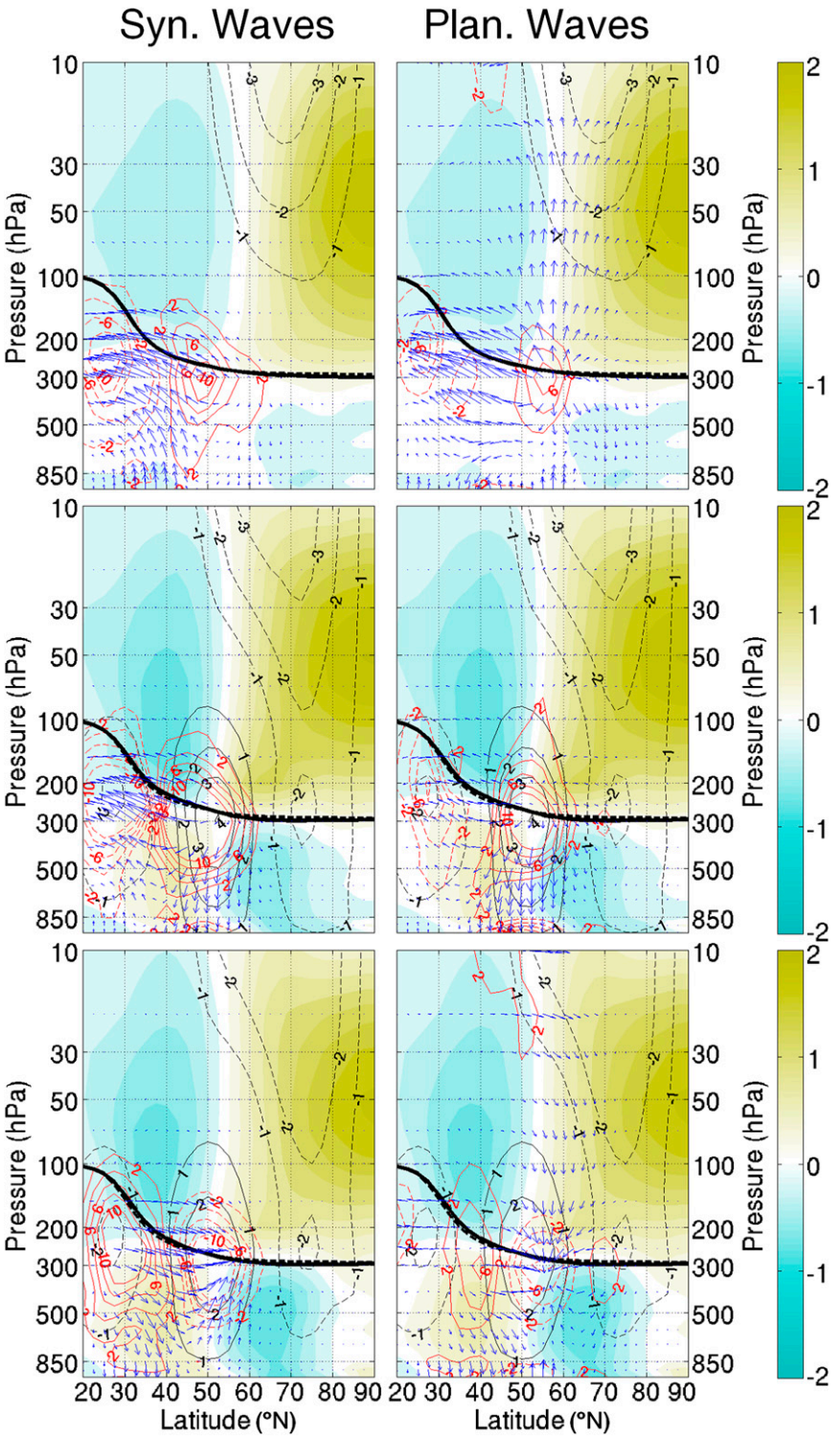

FIG. 3. Lagged composite of PC1 on anomalous EP flux (arrows), anomalous EP flux divergence ($\times 10^{14}\,\mathrm{m^2\,s^{-2}}$; red contours), anomalous zonal-mean zonal wind ($\mathrm{m\,s^{-1}}$; black contours), and anomalous zonal-mean temperature (K; colors) for (left) synoptic and (right) planetary waves at lags (top) −4, (middle) −1, and (bottom) +1 days. The climatological (extended winter) and composite tropopause heights are shown with thick dashed and solid lines, respectively. For clarity of representation, the vertical component of the EP vectors has been scaled as a function of pressure using a p^{-3} factor.

from the equivalence of $\nabla \cdot F$ as a northward flux of quasigeostrophic potential vorticity by the eddies $\overline{v'q'}$. Thus, the anomalous EP flux divergence to the north of the extratropical jet is associated with an anomalous northward flux of quasigeostrophic potential vorticity near the tropopause level, which will produce a positive (negative) anomaly of potential vorticity to the north (south) of the $\nabla \cdot F$ anomaly. This is consistent with the rise of the tropopause (negative anomaly of potential vorticity) to the south of the positive $\nabla \cdot F$ anomaly and its depletion (positive anomaly of potential vorticity) to the north. (Note that the maximum in the Eliassen–Palm divergence is collocated with the node of the tropopause EOF.) The relation between potential vorticity anomalies and tropopause height is thus consistent with the classical model of a potential vorticity perturbation at upper levels (Hoskins et al. 1985; Zängl and Wirth 2002) and with the results of the quasigeostrophic theory (Juckes 1994). It is shown in Fig. 4 that the anomaly in the EP flux divergence is dominated by the eddy momentum flux convergence, especially at the tropopause level, for both synoptic and planetary waves.

The dipolar character of the EOF1 pattern is common to several meteorological fields in the Northern Hemisphere. In particular, the anomalous zonal-mean zonal wind field associated with the first EOF of the extratropical tropopause (black contours in Fig. 3) is very similar to the zonal index [see Fig. 3a in Lorenz and Hartmann (2003)] and indeed the correlation between both time series is highly significant (0.67). This is also consistent with our findings that eddy momentum fluxes are more important than eddy heat fluxes for the pattern of Eliassen–Palm divergence associated with the variations in tropopause height. In contrast, the correlation of the leading tropopause PC with the Artic Oscillation (AO) index is much lower (0.26) even though zonal index and Arctic Oscillation are often regarded as the same variability. This may reflect the fact that the AO index includes several types of atmospheric variability [e.g., several patterns of zonal-mean zonal wind variability; see Feldstein and Lee (2014)], which could impact tropopause height in different ways.

The dynamical evolution of the second EOF exhibits some similar features to those described above for the leading EOF (Fig. 5). Anomalous vertical propagation of synoptic waves is initially found on the southern flank of the extratropical jet a few days ahead of the maximum tropopause anomaly. As time evolves, this develops into an anomalous Eliassen–Palm divergence pattern at upper levels characterized by EP flux divergence over the extratropical jet region and convergence on its flanks (but much stronger on the subtropical side). In this manner, the synoptic eddies produce an acceleration of the extratropical jet, mainly at the expense of the subtropical jet. As for the planetary eddies, the dominant feature is a center of large Eliassen–Palm convergence north of 55°N associated with enhanced vertical propagation in the troposphere and weakened propagation into the stratosphere (plausibly because of the anomalously strong stratospheric jet), which conspire to produce strong wave breaking at tropopause levels over that region. This is accompanied by weakened upward propagation of planetary waves on the south, which is associated with a positive Eliassen–Palm divergence anomaly at upper levels over that region. The combined effect of the synoptic and planetary EP fluxes at upper levels is thus a tripolar EP flux divergence anomaly with a positive center around 45°N and negative centers on the south (north) forced predominantly by the synoptic (planetary) eddies. This Eliassen–Palm divergence pattern is consistent with the structure of the tropopause height perturbations in the manner discussed above for the first EOF. Also as before, anomalies in the EP flux divergence are mainly caused by the eddy momentum fluxes (not shown). Finally, for both the synoptic and planetary eddies the eddy forcing reverses and damps the zonal wind anomalies at positive lags.

b. *Forcings of tropopause variability*

The analysis of the EP fluxes and the zonal-mean zonal wind has identified some common factors involved in the development and decay of the perturbations in tropopause height: anomalies in synoptic and planetary wave breaking at tropopause levels and anomalies in the intensity of the stratospheric polar jet. All these factors are associated with potential vorticity changes at upper levels, caused by either the quasigeostrophic potential vorticity flux associated with wave breaking or the intensification/weakening of the cyclonic circulation at the polar vortex (Ambaum and Hoskins 2002), and may thus be regarded as forcings of tropopause variability. To study the impact of each of these forcings on tropopause height, three indices are constructed by regressing the relevant field on the tropopause PC and projecting this map again onto the field, so that a time series is obtained. The anomalous EP flux divergence between 600 and 100 hPa is used for both synoptic and planetary waves, while the zonal-mean zonal wind between 100 and 10 hPa and 50°–80°N is used as a measure of polar vortex intensity. Note that we regard changes in the polar vortex and changes in the divergence of the planetary EP flux as two different forcings even though changes in the polar vortex affect planetary wave propagation, as described above. We do so because their correlation is low (not shown). Changes in stratospheric propagation only represent a small contribution to the

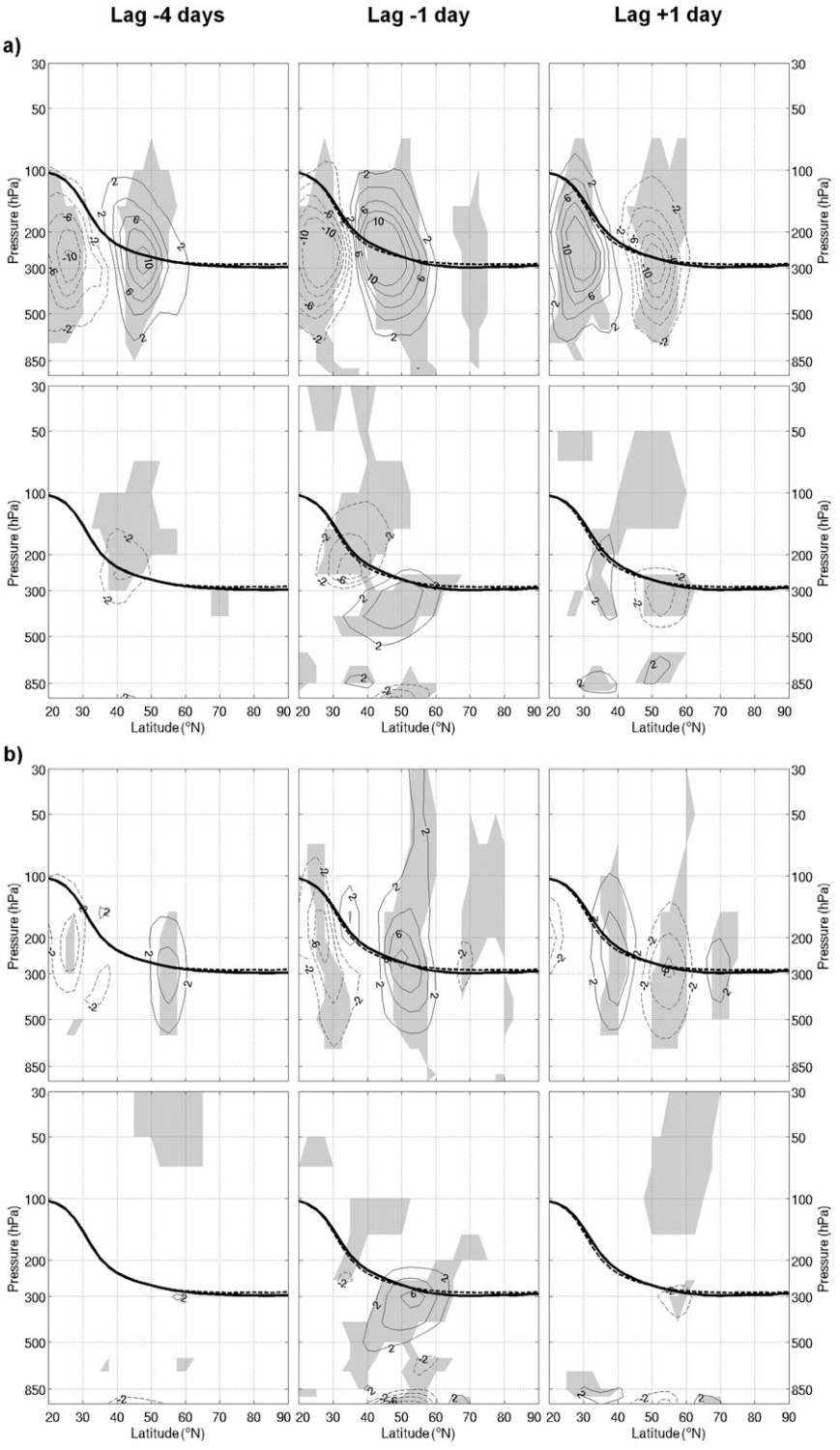

FIG. 4. Lagged composite of PC1 on the components of the EP flux divergence for (a) synoptic and (b) planetary waves. In each case, (top) meridional and (bottom) vertical divergence is shown at lags (left) −4, (center) −1, and (right) +1 days. Contours are labeled every $2 \times 10^{14}\,\mathrm{m^2\,s^{-2}}$ and shading represents areas where the component of the EP flux divergence is statistically different from its mean at 99%. The climatological (extended winter) and composite tropopause heights are shown with thick dashed and solid lines, respectively.

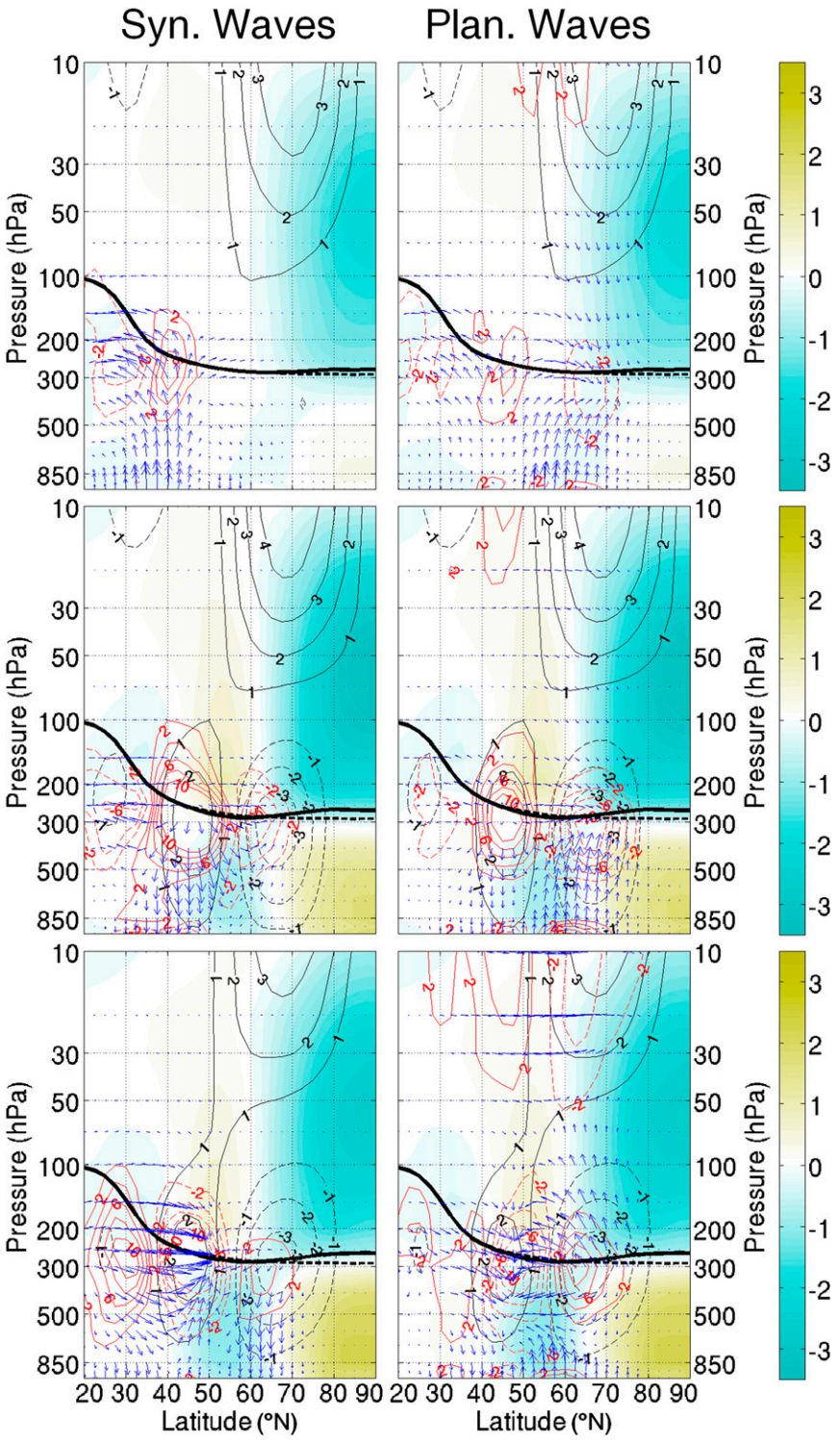

FIG. 5. As in Fig. 3, but for the second EOF, PC2.

full planetary EP flux divergence at tropopause levels, which is dominated by tropospheric dynamics.

It can be seen in Fig. 6 that both modes of tropopause variability are correlated in a similar way with the indices of EP flux divergence, with positive correlations for negative lags (especially from lag −7 to lag −1 days) and weak negative correlations for positive lags. As for the polar vortex index, this index is positively correlated

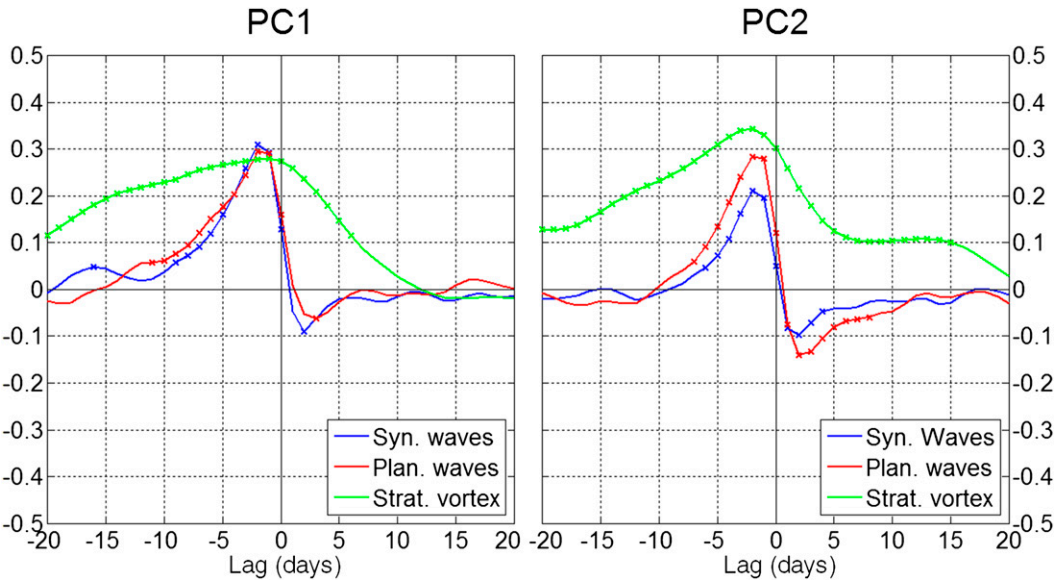

FIG. 6. Lagged correlations between the PCs and the indices described in the text representing tropopause forcings by the synoptic and planetary EP divergence and by the changes in the stratospheric polar vortex. Statistically significant correlations are emphasized using crosses.

with the PC on a longer time scale (over 20 and 40 days for the first and second modes, respectively; full range not shown), with the correlation peaking several days before lag 0. This suggests that the anomalous wave breaking that causes the variations in tropopause height develops in a preexisting anomalous polar vortex while the perturbations (both in tropopause height and in the stratospheric jet) are damped by the waves for positive lags. Figure 7 shows the latitudinal structure of the tropopause anomalies associated with each of these indices, obtained using regression. We can see that while anomalies in the EP flux divergence are usually associated with tropopause anomalies in midlatitudes, the polar vortex index mainly captures the rising or sinking of the polar and subpolar tropopause. The combination of both effects results in the observed EOF (the dashed line in Fig. 7 shows the sum of the tropopause height changes associated to each of these forcings).

Given the different forcing time scales by the waves and the polar vortex, it is worth studying the modes of

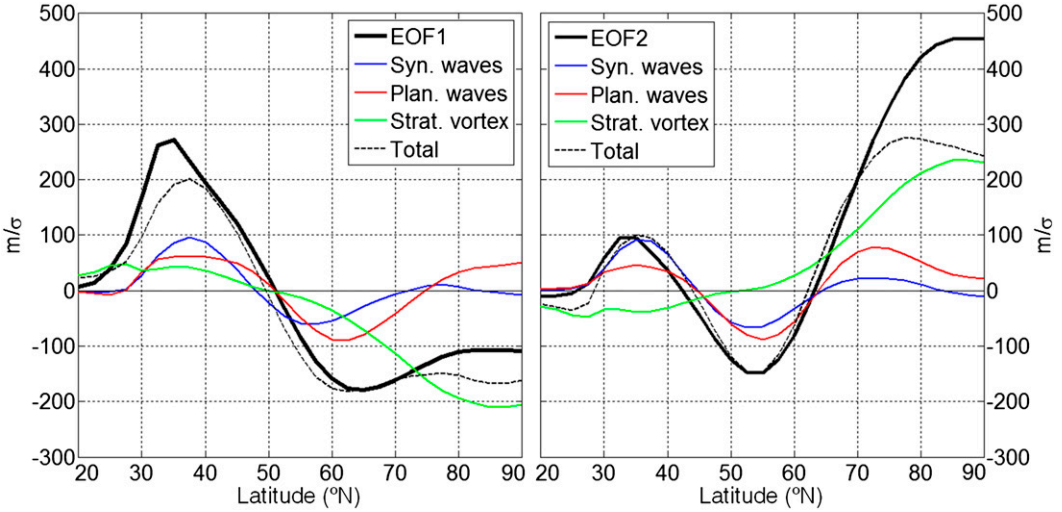

FIG. 7. Tropopause height changes associated with a standard deviation of each of the forcings in Fig. 6 (and their sum, dashed), compared with the full tropopause changes (per standard deviation of the PC).

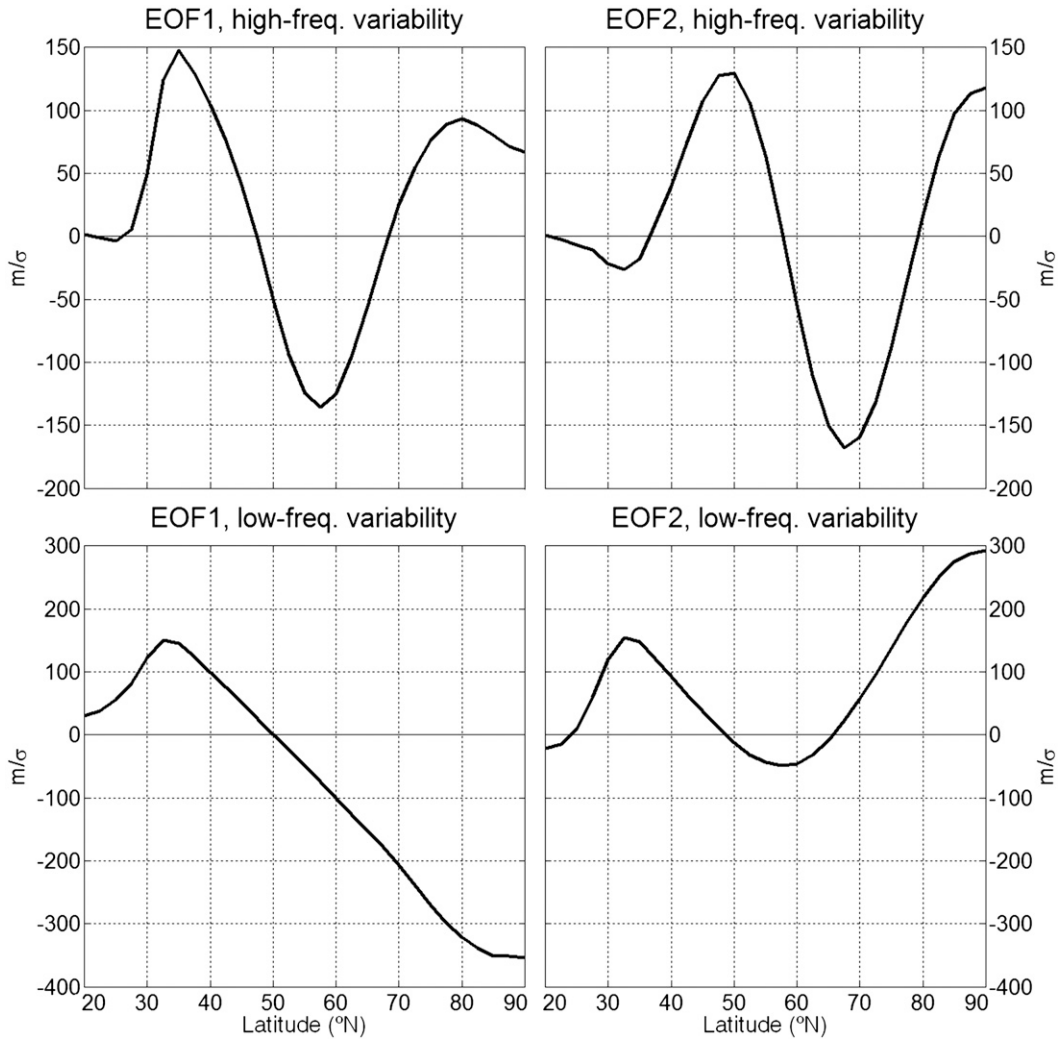

FIG. 8. First two EOFs of the extratropical zonal-mean tropopause height for (top) high- and (bottom) low-frequency intraseasonal variability. See text for details.

tropopause variability on short and long time scales. This was done filtering the data using a high-pass filter with cutoff 1/20 day^{-1} and a low-pass filter with cutoff 1/60 day^{-1}, respectively (the results are robust with other cutoff choices). It can be seen in Fig. 8 that the high-frequency variability of the tropopause is characterized by undulated patterns with maxima and minima of similar amplitude, while low-frequency variability consists mainly in a rising or sinking of the polar tropopause, with a secondary maximum at subtropical latitudes. This is what would be expected when the wave forcing dominates on short time scales, with the associated quasigeostrophic potential vorticity flux inducing a tropopause height dipole around the location of the anomalous wave breaking, and the polar vortex forcing dominates on long time scales, driving variations on the polar and subpolar tropopause on those time scales. The intraseasonal EOFs may be regarded as a combination of both forcings.

5. EOFs of the SH tropopause

To investigate the mechanisms responsible for the variability of the Southern Hemisphere zonal-mean tropopause, PC analysis was performed over the extratropical region from 32.5° to 90°S. As for the NH, the first two modes are well separated, but the first mode now explains more variance than before (35%, compared to 21% for the second one). The first mode again has a dipole pattern (Fig. 9a), with a node at 55°S and extrema at 45° and 80°S; in this case, the southernmost maximum is farther south than that of the SH zonal

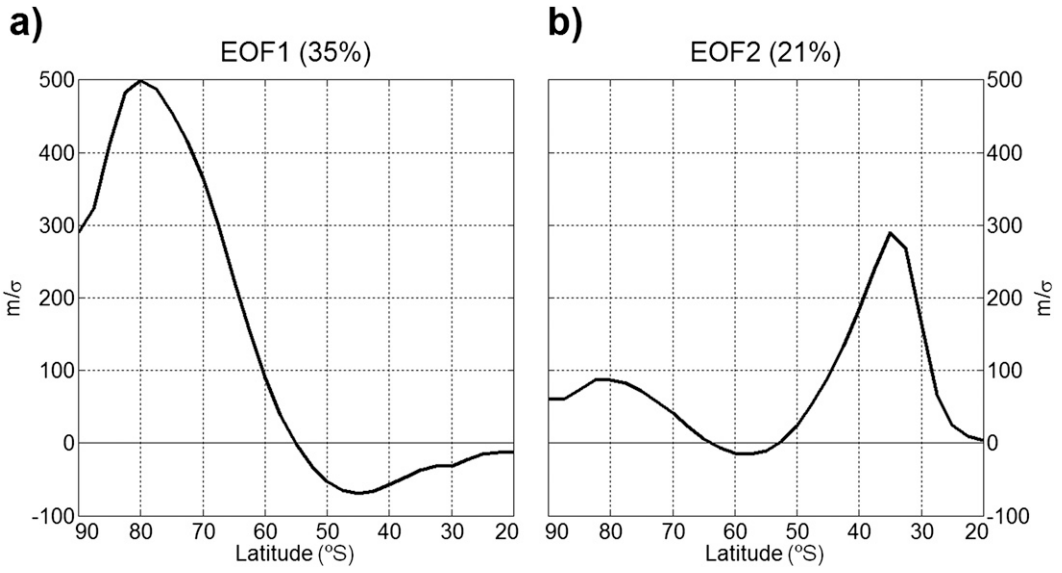

FIG. 9. Regression maps of anomalous zonal-mean tropopause height (m) on (a) PC1 and (b) PC2, for the SH.

index (Lorenz and Hartmann 2001). The second mode (Fig. 9b) consists of two maxima, located at 35° and 80°S. The two modes have similar latitudinal structure except that tropopause anomalies in the mid- and high latitudes are negatively correlated for the first mode and positively correlated for the second mode. Lag-correlation analysis between the associated principal component time series suggests that the two modes of variability may not be independent, as there is a positive correlation when PC1 leads by 10–20 days (Fig. 10).

The dynamical evolution of these modes is described in Fig. 11. As before, tropopause anomalies in the midlatitudes can be linked to changes in the Eliassen–Palm divergence at tropopause levels resulting from changes in wave propagation (note that we no longer distinguish between synoptic and planetary waves, as the former dominate). For the first mode we observe a dipolar EP pattern in the midlatitude upper troposphere, with Eliassen–Palm divergence (convergence) on the equatorward (poleward) side of the jet. This pattern is initially driven by changes in meridional propagation at upper levels and subsequently reinforced by anomalous vertical propagation. The second mode is also associated with a dipolar EP-divergence pattern at upper levels (with the opposite polarity, as defined here), but the pattern is shifted equatorward and the wave driving is different from before. The tropopause anomaly is now initiated by enhanced baroclinic generation and Eliassen–Palm convergence in the subtropics. Finally, large tropopause anomalies are also observed over the polar region for both modes. Although the zonal wind anomalies are weak, significant changes in the vortex potential vorticity are found for these events (not shown), similar to the Northern Hemisphere.

6. Discussion

This work has analyzed the structure and dynamics of the leading modes of variability for the Northern Hemisphere extratropical zonal-mean tropopause height in

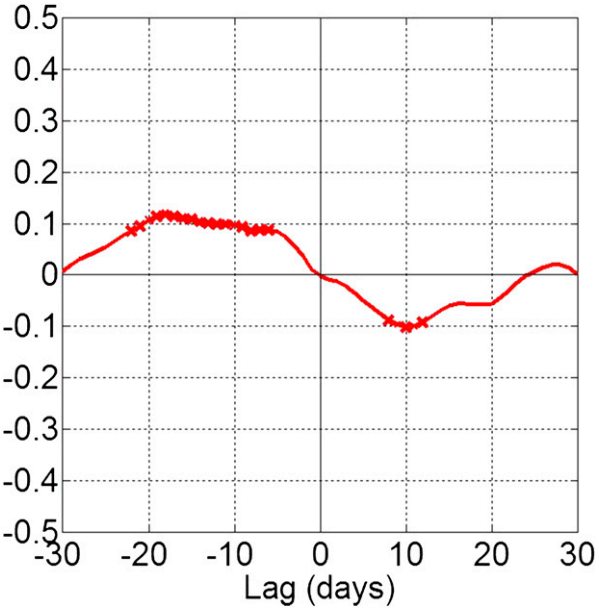

FIG. 10. Lagged correlation between PC1 and PC2 for the SH. PC1 leads (lags) PC2 for negative (positive) lags. Statistically significant correlations are emphasized using crosses.

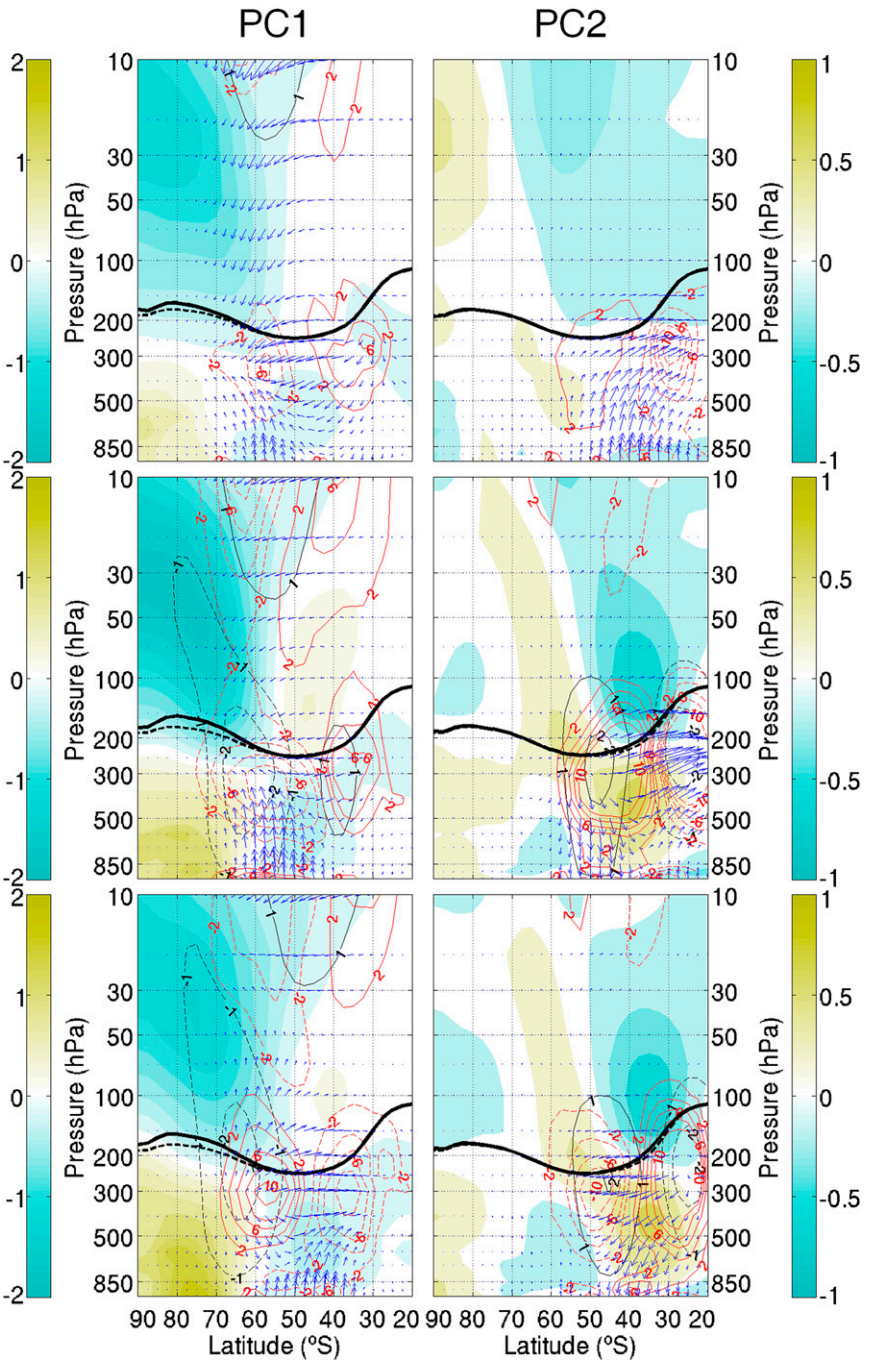

FIG. 11. Lagged composite of (left) PC1 and (right) PC2 on anomalous EP flux (arrows) and anomalous EP flux divergence ($\times 10^{14}\,\mathrm{m^2\,s^{-2}}$; red contours) by all waves, anomalous zonal-mean zonal wind ($\mathrm{m\,s^{-1}}$; black contours), and anomalous zonal-mean temperature (colors) at lags (top) −4, (middle) −1, and (bottom) +1 days. The climatological (extended winter) and composite tropopause heights are shown with thick dashed and solid lines, respectively. For clarity of representation, the vertical component of the EP vectors has been scaled as a function of pressure using a p^{-3} factor.

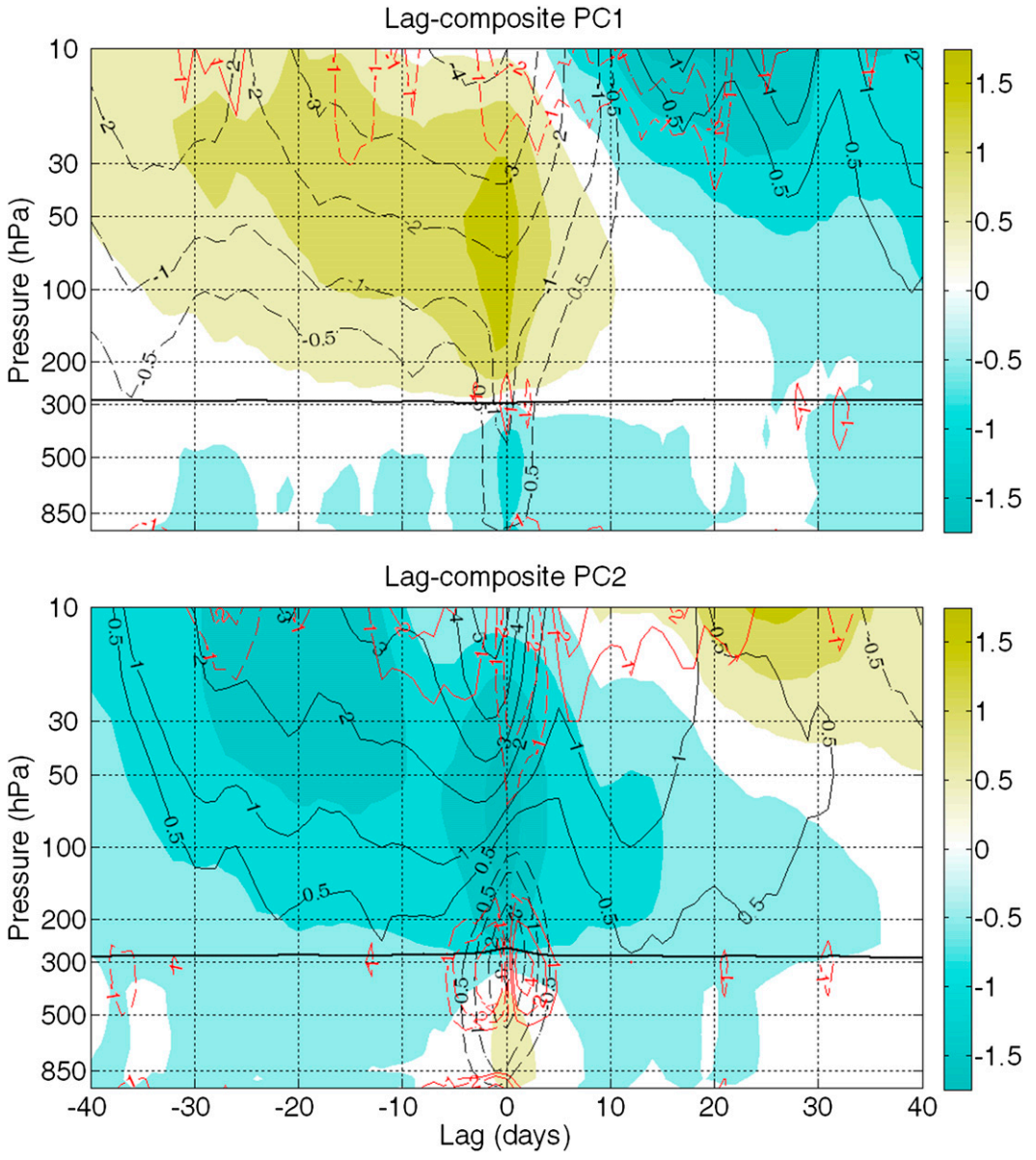

FIG. 12. Lagged composite of (top) PC1 and (bottom) PC2 on anomalous zonal-mean temperature (K; colors), anomalous zonal-mean zonal wind ($m\,s^{-1}$; black contours), and anomalous planetary EP flux divergence ($\times 10^{14}\,m^2\,s^{-2}$; red contours) integrated from 60° to 90°N. Negative contours are indicated as dashes. The thick black solid line represents the lagged composite on the zonal-mean tropopause pressure averaged from 65° to 90°N.

intraannual time scales. The leading mode has a dipolar structure with a node in the midlatitudes and is strongly correlated with the zonal index. The second mode has a tripolar structure and large amplitude over the polar and subpolar regions. The structure of both modes is robust against changes in the latitudinal and temporal domains of analysis.

Previous observational studies of the intraseasonal tropopause variability (e.g., Dell'Aquila et al. 2006; Son et al. 2007) were motivated by the general circulation problem and by theoretical arguments relating baroclinic equilibration and tropopause rise (Held 1982; Lindzen 1993; Schneider 2004). In idealized models, these ideas have been found to have some relevance for tropopause height adjustment in the initial value problem (Egger 1995) and for the mean tropopause in forced-dissipative atmospheres (Zurita-Gotor and Vallis 2011, 2013). In contrast, there is increasing evidence that baroclinic eddy equilibration is quantitatively of little importance for the extratropical internal tropopause variability on

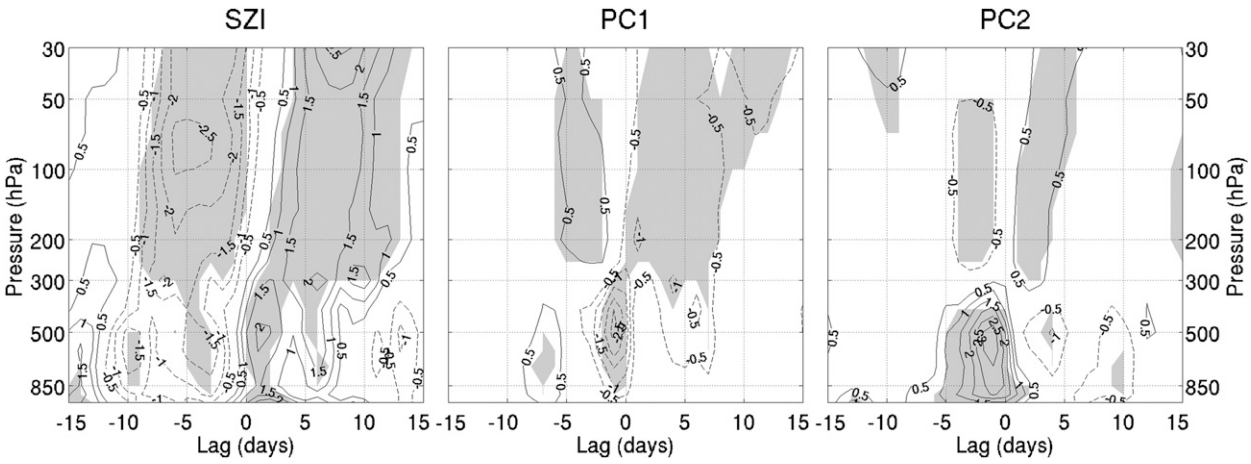

FIG. 13. Lagged composite of the vertical component of Eliassen–Palm flux integrated between 50° and 80°N ($\times 10^{14}$ m^2 s^{-2} Pa) on (left) stratospheric zonal index [SZI; see Limpasuvan et al. (2004) for details], (center) leading mode, and (right) second mode of the zonal-mean extratropical tropopause height variability.

intraseasonal time scales. This was already noted by Son et al. (2007) who found that (i) strong baroclinic life cycles have a small impact on tropopause height and (ii) intense tropopause height events have a large stratospheric signal. Our analysis is consistent with the findings of Son et al. (2007) and provides additional insight on the dynamical forcing of the tropopause variations.

In this regard, the first conclusion of our work is that the dominant modes of zonal-mean tropopause variability are characterized by wavelike patterns with opposite-sign anomalies over different latitudinal bands—that is, with tropopause deformations rather than changes in the extratropical-mean tropopause height. Aiming to find a connection between baroclinic equilibration and tropopause height, we have also computed an index for the extratropical-mean tropopause height and calculated the leading modes of tropopause deformations (changes in tropopause height relative to its time-dependent extratropical mean) at different time scales. We found (results not shown in this paper) that changes in the extratropical-mean tropopause height explain a very small fraction of the full tropopause variability (roughly 20% of the leading EOF variance) and that the leading EOFs of tropopause deformations are nearly indistinguishable from the full EOFs described here. Additionally, we found that changes in the extratropical-mean tropopause are typically associated with large local changes in the subtropical and/or polar tropopause, with weak midlatitude changes.

Based on the thermal definition, it is natural to interpret the tropopause deformations from a heat budget perspective. In particular, the anomalous vertical propagation of synoptic and planetary waves in the upper-troposphere/lower-stratosphere region will produce an anomalous dipole in potential temperature associated with the horizontal eddy heat flux convergence (or, equivalently, the residual vertical velocity). The mechanism is well described by Egger (1995) using a baroclinic channel and was also observed by Dell'Aquila et al. (2006) in actual data. Because planetary waves can propagate more easily at upper levels and/or into the stratosphere (Charney and Drazin 1961), they may have a larger impact on tropopause height than synoptic waves as found by Son et al. (2007).

Alternatively, one could use a potential vorticity framework to understand the tropopause deformations (Hoskins et al. 1985; Zängl and Wirth 2002). Despite the well-known limitations of quasigeostrophic theory for dealing with tropopause dynamics [see, e.g., Song and Nakamura (2000)], a clear link was found in this work between the structure of the tropopause changes and the sign of the anomalous quasigeostrophic potential vorticity flux. The modes of tropopause variability obtained here are associated with the enhancement/weakening of wave breaking at tropopause levels, which produces a southward/northward eddy flux of potential vorticity. A negative eddy PV flux is associated with a positive (negative) PV tendency to the south (north) of the enhanced wave breaking and thus with a tropopause drop (rise), while the opposite is true for a positive eddy PV flux/reduced wave breaking. The quasigeostrophic diagnostics provide a simple conceptual framework for interpreting the changes in wave breaking and associated tropopause deformations in terms of changes in eddy propagation, exploiting the Eliassen–Palm theorem (Edmon et al. 1980). We found that synoptic and planetary waves produce comparable contributions to the Eliassen–Palm divergence for the leading two modes. Additionally, we found that the eddy momentum flux convergence is the

dominant term in the anomalous Eliassen–Palm divergence, particularly for the first EOF, which is strongly connected with zonal index variability (Lorenz and Hartmann 2003).

Both modes of tropopause variability also exhibit a large polar signature. Changes in the polar and subpolar tropopause are associated with changes in the strength of the stratospheric jet that are consistent with the mechanism described by Ambaum and Hoskins (2002). Since isentropic surfaces bend toward cyclonic potential vorticity anomalies (Hoskins et al. 1985), a strong (weak) polar vortex is associated with a rise (drop) in the polar tropopause. The characteristic time scale of polar vortex changes is much longer than that associated with synoptic and planetary wave breaking at tropopause levels, so that persistent stratospheric wind anomalies can be observed well in advance of the EP-divergence anomalies. We can cleanly separate both influences on tropopause height filtering the data.

Although we have not analyzed in this study the source of the preexisting polar vortex anomalies, these resemble the patterns associated with the polar-jet oscillation (PJO; Kodera et al. 2000) and the life cycle of sudden stratospheric warmings (SSW; Limpasuvan et al. 2004). In this regard, significant correlations are found for both PC1 and PC2 with the leading mode of variability of the zonal-mean zonal wind at 50 hPa (stratospheric zonal index), peaking at lags from −7 to −4 days (0.29 for PC1, −0.34 for PC2). Figure 12 shows the downward propagation of stratospheric temperature and wind anomalies as well as the change in phase characteristic of the polar jet vacillations [cf. Fig. 4 of Limpasuvan et al. (2004)] during the development and decay of the tropopause modes. In contrast, the tropospheric evolution of the tropopause modes is very different from that of SSWs. Instead of the downward propagation of the temperature anomalies down to the troposphere observed during the mature stages of SSWs (Limpasuvan et al. 2004), temperature anomalies reverse sign across the tropopause for our modes. This difference highlights the role of the upper-level EP flux divergence (i.e., vertical changes in meridional eddy heat flux/vertical EP flux) for driving the tropopause anomalies, in contrast with the more vertically uniform EP flux anomalies observed during SSWs (Fig. 13). In a similar manner, the convergence of the meridional eddy momentum flux associated with EP flux divergence at tropopause levels causes tropospheric zonal wind perturbations that are not observed during SSWs.

Acknowledgments. This work was supported by the COMETH project (Grant CGL2013-30641) of the Ministerio de Economía y Competitividad of Spain. We are grateful to two anonymous reviewers for their constructive comments.

REFERENCES

Ambaum, M. H. P., and B. J. Hoskins, 2002: The NAO troposphere–stratosphere connection. *J. Climate*, **15**, 1969–1978, doi:10.1175/1520-0442(2002)015<1969:TNTSC>2.0.CO;2.

Andrews, D. G., J. R. Holton, and C. B. Leovy, 1987: *Middle Atmosphere Dynamics*. International Geophysics Series, Vol. 40, Academic Press, 489 pp.

Appenzeller, C., J. R. Holton, and K. H. Rosenlof, 1996: Seasonal variation of mass transport across the tropopause. *J. Geophys. Res.*, **101**, 15 071–15 078, doi:10.1029/96JD00821.

Bethan, S., G. Vaughan, and S. J. Reid, 1996: A comparison of ozone and thermal tropopause heights and the impact of tropopause definition on quantifying the ozone content of the troposphere. *Quart. J. Roy. Meteor. Soc.*, **122**, 929–944, doi:10.1002/qj.49712253207.

Birner, T., 2010: Residual circulation and tropopause structure. *J. Atmos. Sci.*, **67**, 2582–2600, doi:10.1175/2010JAS3287.1.

Bordi, I., A. Dell'Aquila, A. Speranza, and A. Sutera, 2004: On the mid-latitude tropopause height and the orographic–baroclinic adjustment theory. *Tellus*, **56**, 278–286, doi:10.1111/j.1600-0870.2004.00065.x.

Bretherton, C. S., M. Widmann, V. P. Dymnikov, J. M. Wallace, and I. Bladé, 1999: The effective number of spatial degrees of freedom of a time-varying field. *J. Climate*, **12**, 1990–2009, doi:10.1175/1520-0442(1999)012<1990:TENOSD>2.0.CO;2.

Charney, J. G., and P. G. Drazin, 1961: Propagation of planetary-scale disturbances from the lower into the upper atmosphere. *J. Geophys. Res.*, **66**, 83–109, doi:10.1029/JZ066i001p00083.

Davis, N. A., and T. Birner, 2013: Seasonal to multidecadal variability of the width of the tropical belt. *J. Geophys. Res. Atmos.*, **118**, 7773–7787, doi:10.1002/jgrd.50610.

Dell'Aquila, A., P. M. Ruti, and A. Sutera, 2006: Effects of the baroclinic adjustment on the tropopause in the NCEP–NCAR reanalysis. *Climate Dyn.*, **28**, 325–332, doi:10.1007/s00382-006-0199-4.

Edmon, H. J., Jr., B. J. Hoskins, and M. E. McIntyre, 1980: Eliassen–Palm cross sections for the troposphere. *J. Atmos. Sci.*, **37**, 2600–2616, doi:10.1175/1520-0469(1980)037<2600:EPCSFT>2.0.CO;2.

Egger, J., 1995: Tropopause height in baroclinic channel flow. *J. Atmos. Sci.*, **52**, 2232–2241, doi:10.1175/1520-0469(1995)052<2232:THIBCF>2.0.CO;2.

Feldstein, S. B., and S. Lee, 2014: Intraseasonal and interdecadal jet shifts in the Northern Hemisphere: The role of warm pool tropical convection and sea ice. *J. Climate*, **27**, 6497–6518, doi:10.1175/JCLI-D-14-00057.1.

Held, I. M., 1982: On the height of the tropopause and the static stability of the troposphere. *J. Atmos. Sci.*, **39**, 412–417, doi:10.1175/1520-0469(1982)039<0412:OTHOTT>2.0.CO;2.

Hoinka, K. P., 1998: Statistics of the global tropopause pressure. *Mon. Wea. Rev.*, **126**, 3303–3325, doi:10.1175/1520-0493(1998)126<3303:SOTGTP>2.0.CO;2.

Holton, J. R., P. H. Haynes, M. E. McIntyre, A. R. Douglass, R. B. Rood, and L. Pfister, 1995: Stratosphere–troposphere exchange. *Rev. Geophys.*, **33**, 403–439, doi:10.1029/95RG02097.

Hoskins, B. J., M. E. McIntyre, and A. W. Robertson, 1985: On the use and significance of isentropic potential vorticity maps. *Quart. J. Roy. Meteor. Soc.*, **111**, 877–946, doi:10.1002/qj.49711147002.

Juckes, M., 1994: Quasigeostrophic dynamics of the tropopause. *J. Atmos. Sci.*, **51**, 2756–2768, doi:10.1175/1520-0469(1994)051<2756:QDOTT>2.0.CO;2.

——, 2000: The static stability of the midlatitude troposphere: The relevance of moisture. *J. Atmos. Sci.*, **57**, 3050–3057, doi:10.1175/1520-0469(2000)057<3050:TSSOTM>2.0.CO;2.

Kodera, K., Y. Kuroda, and S. Pawson, 2000: Stratospheric sudden warmings and slowly propagating zonal-mean zonal wind anomalies. *J. Geophys. Res.*, **105**, 12 351–12 359, doi:10.1029/2000JD900095.

Limpasuvan, V., D. W. J. Thompson, and D. L. Hartmann, 2004: The life cycle of the Northern Hemisphere sudden stratospheric warmings. *J. Climate*, **17**, 2584–2596, doi:10.1175/1520-0442(2004)017<2584:TLCOTN>2.0.CO;2.

Lindzen, R. S., 1993: Baroclinic neutrality and the tropopause. *J. Atmos. Sci.*, **50**, 1148–1151, doi:10.1175/1520-0469(1993)050<1148:BNATT>2.0.CO;2.

Lorenz, D. J., and D. L. Hartmann, 2001: Eddy–zonal flow feedback in the Southern Hemisphere. *J. Atmos. Sci.*, **58**, 3312–3327, doi:10.1175/1520-0469(2001)058<3312:EZFFIT>2.0.CO;2.

——, and ——, 2003: Eddy–zonal flow feedback in the Northern Hemisphere winter. *J. Climate*, **16**, 1212–1227, doi:10.1175/1520-0442(2003)16<1212:EFFITN>2.0.CO;2.

North, G. R., T. L. Bell, R. F. Cahalan, and F. J. Moeng, 1982a: Sampling errors in the estimation of empirical orthogonal functions. *Mon. Wea. Rev.*, **110**, 699–706, doi:10.1175/1520-0493(1982)110<0699:SEITEO>2.0.CO;2.

——, F. J. Moeng, T. L. Bell, and R. F. Cahalan, 1982b: The latitude dependence of the variance of zonally averaged quantities. *Mon. Wea. Rev.*, **110**, 319–326, doi:10.1175/1520-0493(1982)110<0319:TLDOTV>2.0.CO;2.

Reed, R. J., 1955: A study of a characteristic type of upper level frontogenesis. *J. Meteor.*, **12**, 226–237, doi:10.1175/1520-0469(1955)012<0226:ASOACT>2.0.CO;2.

Reichler, T., M. Dameris, and R. Sausen, 2003: Determining the tropopause height from gridded data. *Geophys. Res. Lett.*, **30**, 2042, doi:10.1029/2003GL018240.

Schneider, T., 2004: The tropopause and the thermal stratification in the extratropics of a dry atmosphere. *J. Atmos. Sci.*, **61**, 1317–1340, doi:10.1175/1520-0469(2004)061<1317:TTATTS>2.0.CO;2.

Seidel, D. J., and W. J. Randel, 2006: Variability and trends in the global tropopause estimated from radiosonde data *J. Geophys. Res.*, **111**, D21101, doi:10.1029/2006JD007363.

Shepherd, T. G., 2002: Issues in stratosphere–troposphere coupling. *J. Meteor. Soc. Japan*, **80**, 769–792, doi:10.2151/jmsj.80.769.

Son, S., S. Lee, and S. B. Feldstein, 2007: Intraseasonal variability of the zonal-mean extratropical tropopause height. *J. Atmos. Sci.*, **64**, 608–620, doi:10.1175/JAS3855.1.

Song, Y., and N. Nakamura, 2000: Eady instability of isolated baroclinic jets with meridionally varying tropopause height. *J. Atmos. Sci.*, **57**, 46–65, doi:10.1175/1520-0469(2000)057<0046:EIOIBJ>2.0.CO;2.

Thompson, D. W. J., and J. M. Wallace, 2000: Annular modes in the extratropical circulation. Part I: Month-to-month variability. *J. Climate*, **13**, 1000–1016, doi:10.1175/1520-0442(2000)013<1000:AMITEC>2.0.CO;2.

Thuburn, J., and G. C. Craig, 1997: GCM tests of theories for the height of the tropopause. *J. Atmos. Sci.*, **54**, 869–882, doi:10.1175/1520-0469(1997)054<0869:GTOTFT>2.0.CO;2.

——, and G. Craig, 2000: Stratospheric influence on tropopause height: The radiative constraint. *J. Atmos. Sci.*, **57**, 17–28, doi:10.1175/1520-0469(2000)057<0017:SIOTHT>2.0.CO;2.

Wittman, M. H., A. J. Charlton, and L. M. Polvani, 2005: On the meridional structure of annular modes. *J. Climate*, **18**, 2119–2122, doi:10.1175/JCLI3394.1.

WMO, 1957: Definition of the tropopause. *WMO Bull.*, **6**, 136.

Wong, S., and W.-C. Wang, 2003: Tropical–extratropical connection in interannual variation of the tropopause: Comparison between NCEP/NCAR reanalysis and an atmospheric general circulation model simulation. *J. Geophys. Res.*, **108**, 4043, doi:10.1029/2001JD002016.

Wu, Y., and O. Pauluis, 2014: Midlatitude tropopause and low-level moisture. *J. Atmos. Sci.*, **71**, 1187–1200, doi:10.1175/JAS-D-13-0154.1.

Zängl, G., and V. Wirth, 2002: Synoptic-scale variability of the polar and subpolar tropopause: Data analysis and idealized PV inversions. *Quart. J. Roy. Meteor. Soc.*, **128**, 2301–2315, doi:10.1256/qj.01.76.

Zurita-Gotor, P., and G. K. Vallis, 2011: Dynamics of midlatitude tropopause height in an idealized model. *J. Atmos. Sci.*, **68**, 823–838, doi:10.1175/2010JAS3631.1.

——, and ——, 2013: Determination of extratropical tropopause height in an idealized gray radiation model. *J. Atmos. Sci.*, **70**, 2272–2292, doi:10.1175/JAS-D-12-0209.1.